Soft Matter

Accepted Manuscript

ROYAL SOCIETY OF CHEMISTRY

www.rsc.org/softmatter

Cite this: DOI: 10.1039/c0xx00000x

www.rsc.org/xxxxxx

ARTICLE TYPE

Directed Self-Assembly of Solvent-Vapor-Induced Non-Bulk Block Copolymer Morphologies on Nanopatterned Substrates

Lei Wan,[a] Shengxiang Ji,[b] Chi-Chun Liu,[c] Gordon S.W. Craig,[d] and Paul F. Nealey*[d]

Received (in XXX, XXX) Xth XXXXXXXXX 200X, Accepted Xth XXXXXXXXX 200X

DOI: 10.1039/b000000x

We report a study on directed self-assembly (DSA) with solvent annealing to induce the formation of non-bulk block copolymer microdomains on chemical patterns. Ultrathin films of symmetric polystyrene-*block*-poly(methyl methacrylate) (PS-*b*-PMMA) display morphologies of PMMA dots, stripes, and PS hexagons with increasing exposure time to acetone vapor, a PMMA-selective solvent. All three nanostructures form long-range-ordered and registered arrays on striped chemical patterns with periods (L_s) commensurate to the solvated PS-*b*-PMMA microdomain period ($L_{0,s}$). Solvent annealing is shown to facilitate DSA on non-regular chemical patterns, on which the local periods are incommensurate to $L_{0,s}$. DSA with feature density mulitplication, via solvent annealing, is also demonstrated.

Introduction

Directed self-assembly (DSA) of thin films of block copolymer (BCP) is a promising method for further improving resolution and throughput in nanolithography.[1-3] DSA relies on the thermodynamically driven microphase separation of BCPs to generate uniform, periodic arrays of nanostructures with typical dimensions of 3-50 nm.[4] The type of nanostructure that forms naturally (e.g. cylinders, spheres, or lamelle) and their natural spacing period L_0 depend on the BCP's Flory-Huggins interaction parameter (χ), degree of polymerization (N), and block volume fraction (f).[4] Self-assembly of these nanostructures can be guided by chemical[5-14] or topographical[15-18] templates to form long-range ordered and registered patterns, which are essential for the fabrication of bit-patterned media (BPM)[19, 20] and semiconductor devices.[2, 21-23] DSA of a thin film of BCP is generally limited to forming patterns with fixed dimensions and a single geometry, such as close packed dots or lines. Although DSA on chemical patterns can cause a BCP to form structures that differ from its L_0 by up to 10%,[6] typically in order to obtain a different pattern geometry and/or size, synthesis of a different polymer is required to change the chemistry, N, or f of the BCP.

However, if the BCP thin film is annealed by solvent vapor (instead of thermally), its morphology and size can be regulated by the choice of solvent and the amount of solvent present in the BCP during annealing.[24] For example, Bosworth *et al*. showed that the use of a nonselective or a selective solvent in the annealing of thin films poly(α-methylstyrene)-*block*-poly(4-hydroxystyrene) could cause the BCP to form cylinders or sphers, respectively.[25] Similarly, Jung *et al*.[26] reported that the BCP nanostructures can be varied from lamellae to cylinders depending on the solvent used during annealing. Jeong *et al*. demonstrated an extraordinarily large degree of tunability in morphology and dimension of a poly(2-vinylpyridine)-*block*-polydimethylsiloxane thin film.[27] Ober and co-workers achieved the impressive morphological flexiblity with one system when they showed that the use of mixtures of selective solvents to anneal thin films of poly(2-hydroxyethyl methacrylate)-*block*-poly(methyl methacrylate) can controllably yield lameallar, gyroid, cylindrical, and spherical morphologies.[28] Separate research has shown that the self-assembly of the solvent-vapor-annealed BCP microdomains can be directed by both topographical[25, 29-32] and chemical[33-36] patterns.

Studies have also shown that solvent annealing can lead to an evolution of domain structures as the annealing progresses. Recently Wu *et al*. showed a dependence of domain structure on annealing time, and also on solvent evaporation rate, of thin films of gyroid-forming polystyrene-*block*-poly(L-lactide).[37] Similarly, Han and coworkers reported that when an ultrathin film (thickness < L_0/2) of symmetric polystyrene-*block*-poly(methyl methacrylate) (PS-*b*-PMMA) film is annealed in acetone or chloroform vapor, its morphology evolves with increasing annealing time.[38-40] Initially, a PS-rich layer is at the free surface because PS has a lower surface tension than PMMA. Exposure of the film to PMMA-selective solvent vapor causes gradual migration of the PMMA block to the free surface. Due to the strong surface interaction and high molecular weight of the blocks, the dynamics of the phase separation and ordering can be slow enough to allow non-bulk morphologies to be obtained by terminating the solvent annealing processe after a specific time.

Another example of non-bulk morphologies that are needed for technological applications of DSA of BCPs comes from non-regular, device-oriented structures, such as bent lines. Thermally annealed DSA of BCP films has been demonstrated to achieve device-oriented structures.[9, 41-43] One main challenge of DSA on non-regular patterns lies in the presence of local periods that are not commensurate with L_0. For example, the corner-to-corner period (L_c) in bends is much larger than L_0. Previously, defect-free assembly at the bend corners could be obtained either by using an ABA triblock copolymer with extremely large stretchability,[43] or a BCP/homopolymer blend[9] in which the homopolymers can redistribute and facilitate the non-

commensurate DSA.

In this work we build upon the previous work on solvent annealing of BCPs to establish the use of DSA with solvent annealing to form, order, and register non-bulk morphologies on chemical patterns. We demonstrate that these non-bulk structures can be guided on chemically patterned surfaces to generate long-range-ordered and registered patterns. A single BCP/solvent system can be used to form microdomains with a range of structures. Furthermore, we demonstrate that solvent annealing can also facilitate DSA on non-regular chemical patterns, such as bends, by redistributing the solvent molecules. Finally, we show that DSA of solvent-annealed, non-bulk morphologies can accomplish feature density multiplication, as has been previously demonstrated with both thermally annealed[14, 44] and solvent-annealed[34-36] BCP thin films.

Experimental

Materials

Hydroxyl-terminated PS (PS-OH, M_n = 6.0 kg/mol, PDI = 1.07), hydroxyl-terminated PMMA (PMMA-OH, M_n = 6.3 kg/mol, PDI = 1.06), and two different lots of PS-*b*-PMMA (M_n = 52-52, and 95-92 kg/mol, polydispersity index (PDI) = 1.10, and 1.06, respectively), were purchased from Polymer Source Inc. PMMA photoresist (M_n = 950 kg/mol, 4 wt% in chlorobenzene) was purchased from MicroChem Inc. All solvents were purchased from Aldrich and used as received. Hydroxyl-terminated poly(styrene-*rand*-methyl methacrylate) (PS-*r*-PMMA-OH, M_n = 12.5 kg/mol, PDI = 1.25) was synthesized by nitroxide-mediated polymerization according to the reported procedure.[45] The styrene fraction of the PS-*r*-PMMA-OH was determined to be 57 mol% by ^{1}H NMR analysis. Cross-linkable PS (M_n = 30.5 kg/mol, PDI = 1.22) was synthesized by nitroxide-mediated copolymerization of styrene and glycidyl methacrylate and contained ~ 4 mol% of cross-linkable epoxy groups.

Substrate modification

1 wt% toluene solutions of hydroxyl terminated polymers (PS-OH, PMMA-OH, or PS-*r*-PMMA-OH) was spin-coated on silicon wafers and annealed at 190 °C for 7 h under vacuum. The substrates were then sonicated in toluene to remove the non-grafted polymer, which yielded 3-4 nm thick imaging layers. To prepare substrates with a cross-linked PS (XPS) mat, a 0.2 wt % toluene solution of cross-linkable PS was spin-coated on silicon wafers and annealed at 190 °C for 24 h under vacuum. Non-crosslinked PS was removed by sonication in toluene, yielding an XPS mat with a thickness of ~7 nm.

Fabrication of chemical patterns

A 70-nm-thick PMMA photoresist film was deposited onto the silicon substrates grafted with PS-OH or XPS and baked at 160 °C for 60 s. The photoresist patterns were exposed either by electron beam lithography (EBL) or extreme ultra-violet interference lithography (EUV-IL). EBL was performed on a LEO 1550 VP SEM equipped with a J. C. Nabity pattern generation system with an acceleration voltage of 20 kV.[6, 7] EUV-IL was carried out at the Synchrotron Radiation Center (SRC) at the University of Wisconsin-Madison using a transmission membrane interferometric mask.[46] All patterns were exposed on PMMA resist and developed with a 1:3 (v:v) mixture of methyl isobutyl ketone:isopropanol (MIBK:IPA) for 60 s and rinsed with IPA. The 1:1 chemical patterns with alternative stripes of PS-OH (or XPS) and bare SiO_x were obtained by O_2 plasma etching and stripping the photoresist in chlorobenzene with sonication.

1:2 chemical patterns for DSA with feature density mulitplication were fabricated using a process with improved control in chemistry and geometry.[47] Resist patterns were exposed on XPS-grafted substrate. The resist patterns were trimmed by extending the O_2 plasma etching time. After removal of the photoresist with chlorobenzene, a 20-nm-thick film of PS-*r*-PMMA-OH with 50 mol% of styrene content was spin-coated onto the patterned substrate. The substrate was then annealed at 190 °C for 4 h to graft the brush into the interfacial regions between the XPS stripes. Excess PS-*r*-PMMA-OH was removed by sonication in toluene to yield grating patterns of alternating XPS stripes with width of $0.5L_{0,s}$ and PS-*r*-PMMA stripes.

Solvent Annealing

Thin films of PS-*b*-PMMA were spin-coated on the substrates from a 1 wt% toluene solution. The samples were then placed in a sealed 20-mL vial along with an open 5-mL vial containing approximately 2 mL solvent. Solvent annealing was carried out at an ambient temperature of 22 ˚C for 1.5-46 h. Identical vials and solvent containers were used for every experiment. After annealing, the samples were taken out of the vial and dried quickly in ambient atmosphere.

Scanning Electron Microscopy (SEM)

A LEO 1550 VP field-emmisson SEM was used to image the BCP films using 1 kV acceleration voltage. The BCP films were imaged without PMMA block removal unless specified. The PMMA block was removed by exposing to UV light for 10 min, immersing into acetic acid for 2 min, and rinsing with deionized water.

Results

Solvent Selection

To select a solvent for our study in this work, we first tested solvent annealing ultrathin films of PS-*b*-PMMA (95k-*b*-92k) with four different solvents: CS_2, toluene, chlorobenzene, and acetone. Annealing with CS_2 yielded a micellar structure similar to that observed in previous work. Annealing with chlorobenzene or toluene yielded a disordered worm-like morphology (Supplemental Information Figure S1). We selected acetone as our solvent for further study because well-ordered structures were assembled when acetone was used to solvent anneal PS-*b*-PMMA, and because acetone could induce the formation of non-bulk morphologies in PS-*b*-PMMA. The relevant polymer-solvent interaction parameters are $\chi_{PS\text{-}acetone}$ = 1.1 and $\chi_{PMMA\text{-}acetone}$ = 0.29, indicating that acetone has strong selectivity to PMMA.

Morphology Evolution with Annealing Time

The evolution of the BCP morphology with annealing time is shown in Figure 1. We annealed 25-nm-thick PS-*b*-PMMA (95k-*b*-92k) films with acetone vapor on both unpatterned and striped chemical patterns for times ranging from 1.5 h to 46 h. Prior to annealing, top-down SEMs of the as-cast films revealed disordered, worm-like structures (not shown here). Focusing on the unpatterned substrate that was grafted with PS-OH brush (left side of Fig. 1), the BCP film morphology evolved with increasing solvent annealing time. After 1.5 h of solvent annealing, the film became featureless. With additional annealing time, (3 h and 5 h) dots of PMMA were present. 10 h of exposure to acetone vapor resulted in a morphology that at the top surface appeared as a collection of disordered and intertwined linear domains. With continued annealing, the structure evolved into and maintained a honeycomb structure of PS hexagons. A similar trend of the morphological evolution was also observed on unpatterned substrates grafted with $PS_{57\%}$-*r*-PMMA-OH or PMMA-OH (Supporting Information Figure S2). The self-assembled solvent annealing periods ($L_{0,s}$) of the PMMA dots, stripes, and PS hexagons were all approximately 75 nm, as determined by FFT analysis of the SEM images of the domains on unpatterned substrates. In the case of assembled dots and hexagons, $L_{0,s}$ corresponded to the spacing of the lines of domains, and not the domain-domain spacing.

Assembly on a striped chemical pattern, which had pattern period L_S set to 70 nm to be approximately commensuratee with $L_{0,s}$, showed the same evolution of morphology, but also revealed that the assembly of all three of the BCP morphologies could be directed by the underlying chemical pattern (right side of Fig. 1). After 5 h of annealing PS-*b*-PMMA on the chemical pattern, the PMMA dots were aligned with the chemical pattern. Long-range-ordered and well-registered stripes were observed after 10 h annealing. Annealing for 15 h resulted in the mixture of aligned stripes and PS hexagons. Close-packed PS domains formed and aligned with the chemical patterns after annealing for longer times. For each of the morphologies, the assembly of these domains into ordered, linear patterns was possible in part because the characteristic length scales of the pattern (period L_S) and solvated copolymer ($L_{0,s}$) were approximately commensurate.

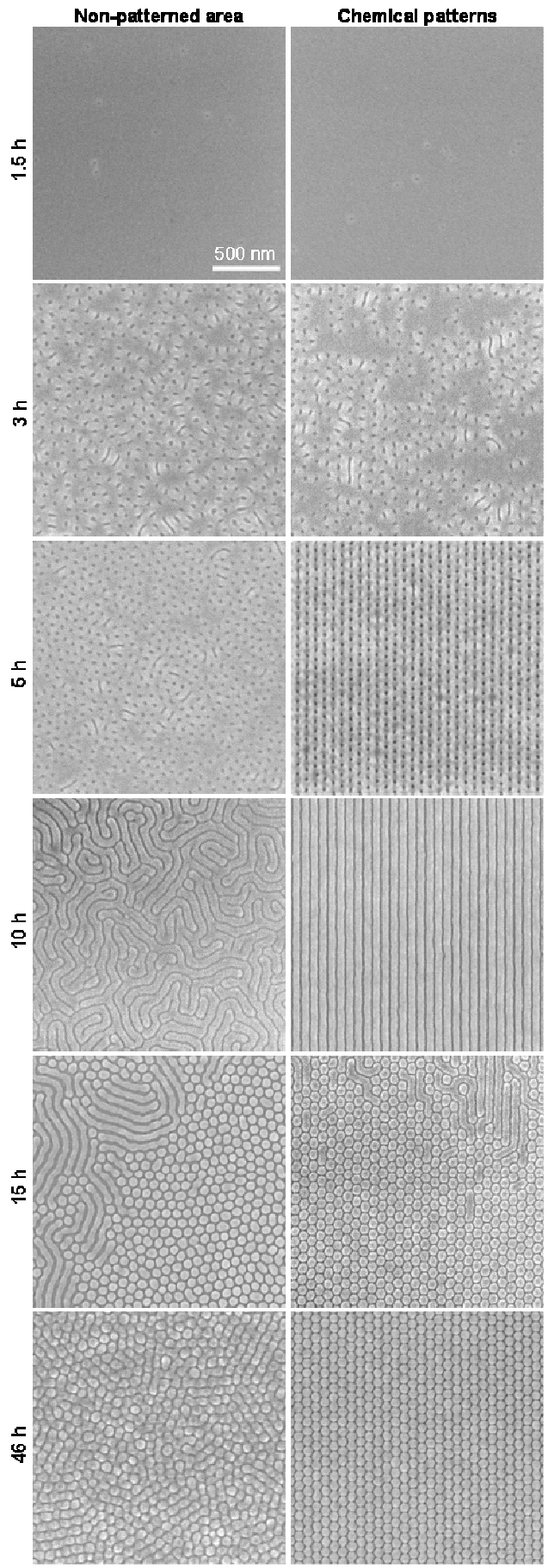

Figure 1: Top-down SEM images of PS-*b*-PMMA (95k-*b*-92k) 25-nm-thick films on non-patterned (left column) and striped chemical patterns with L_S = 70 nm (right column). The films were annealed in acetone vapor for 1.5 - 46 h. Bright regions correspond to PS domains.

DSA of Non-bulk Morphologies on Chemical Patterns

DSA of PMMA dots. An examination of DSA with solvent annealing on chemical patterns with a range of L_S values revealed that DSA of the non-bulk morphologies can occur over a limited range of L_S for a given $L_{0,s}$. Figure 2 shows top-down SEM images of a 25-nm-thick film of PS-*b*-PMMA (95k-*b*-92k) on striped chemical patterns with L_S = 70, 80, and 90 nm after 5 h of annealing in acetone vapor. When L_S was approximately commensurate with $L_{0,s}$ (L_S = 70 and 80 nm), the PMMA dots aligned with a hexagonal arrangement, with lines of dots parallel to chemical pattern stripes. The period between parallel lines of the assembled PMMA dots was equal to L_S. The alignment reveals the guiding of the chemical patterns. The hexagonal ordering of the PMMA dots is apparent in the inset 2D FFT images. In contrast, on chemical patterns with L_S = 90 nm, neither the linear alignment of the PMMA dots nor the hexagonal ordering with their nearest neighbors was present because the disparity between $L_{0,s}$ and L_S was too great for the chemical pattern to direct the assembly of the domains.

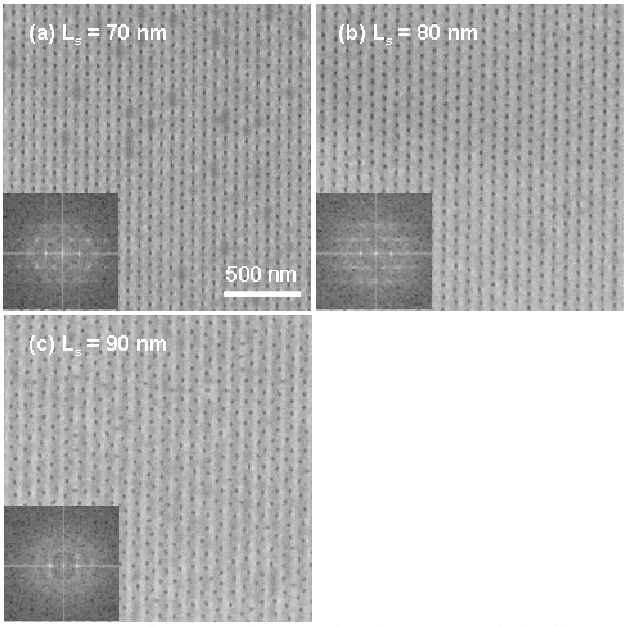

Figure 2. Top-down SEM images of PS-*b*-PMMA (95k-*b*-92k) 25-nm-thick films annealed in acetone vapor for 5h on chemical patterns with L_S = 70 nm (a), L_S = 80 nm (b), and L_S = 90 nm (c). The SEM imaging direction was adjusted so that the stripes of chemical patterns are vertical in the images

DSA of Stripes. The range of L_S values over which the chemical pattern could direct the assembly of PS-*b*-PMMA was more apparent in the DSA of stripes. Figure 3 shows DSA of PS-*b*-PMMA after 10 h of annealing on chemical patterns with L_S = 60-95 nm. On chemical patterns with L_S = 60 and 65 nm (Fig. 3a and b), the period of the assembled striped pattern approximately equaled $L_{0,s}$, and the stripes were partially oriented in the direction of the underlying chemical pattern. Long-range-ordered and registered stripes were observed with periods equal to L_S when L_S = 70, 75, and 80 nm (Fig. 3c-e). With increasing L_S (L_S = 85, 90, and 95 nm), wavy BCP stripe patterns with period equal to $L_{0,s}$ were observed (Fig. 3f-h). As L_S was increased from 85 to 90 and 95 nm, the waviness of the lines became more pronounced, until at 95 nm the lines only minimally followed the general orientation of the underlying chemical pattern. In comparison to DSA of perpendicularly oriented lamellae,[8] DSA of these stripes produced similar pattern quality, but had slightly less commensurability tolerance.

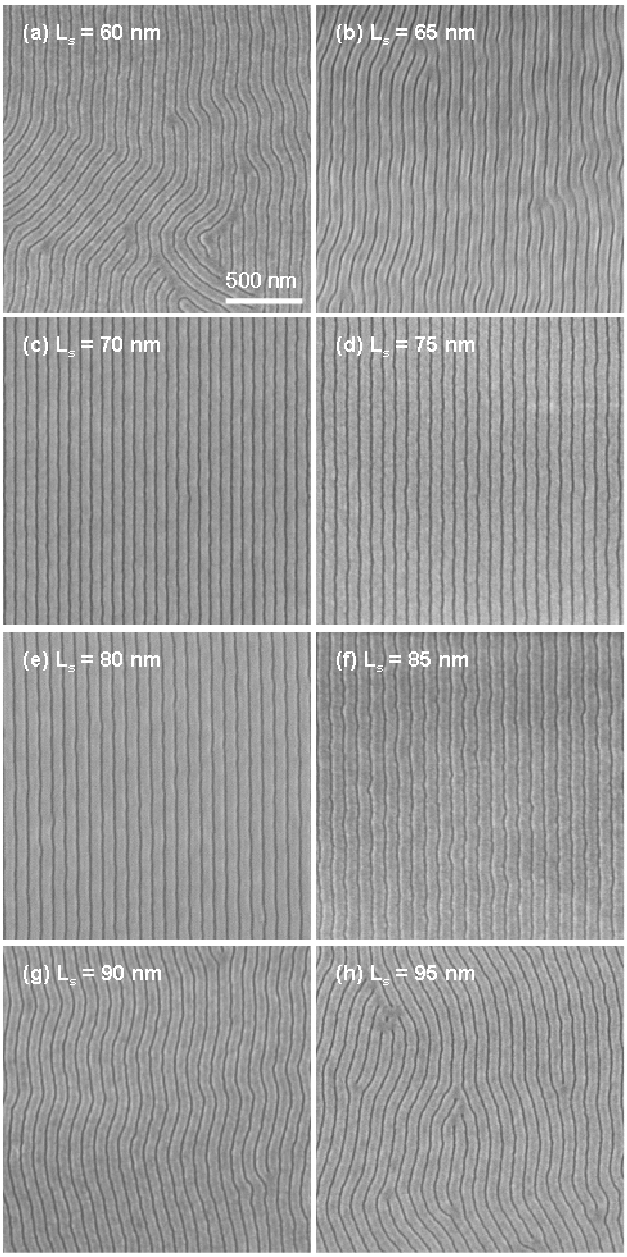

Figure 3. Top-down SEM images of PS-*b*-PMMA (95k-*b*-92k) 25-nm-thick films annealed in acetone vapor for 10h on chemical patterns with L_S = 60-95 nm.

DSA of PS Hexagons. The degree of commensurability of L_S with $L_{0,s}$ had a similar effect on the assembly of the PS hexagons that formed after annealing 25-nm-thick films of PS-*b*-PMMA on striped chemical patterns for 46 h in acetone vapor. On striped chemical patterns with L_S ranging from 60 to 95 nm, all films showed closely packed, hexagonally shaped PS domains, as shown in Figure 4. The period of the lines of assembled hexagons equaled L_S on substrates with $70 \leq L_S \leq 80$. When L_S was outside

this range, the period of the lines of assembled hexagons equaled $L_{0,s}$.

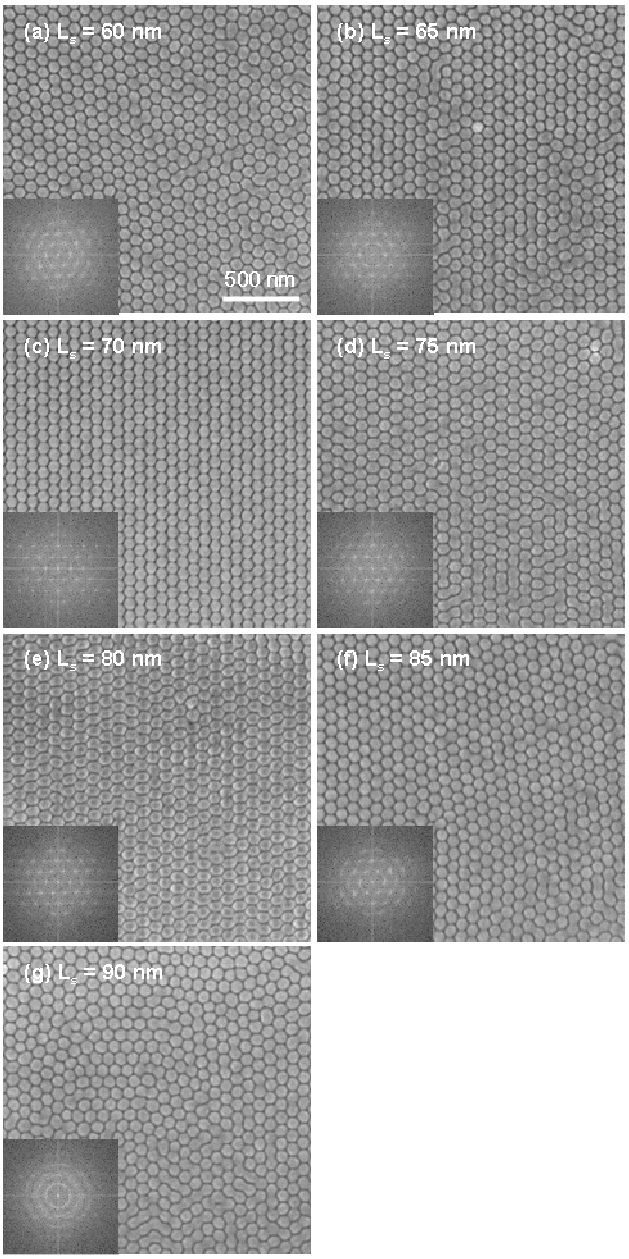

Figure 4. Top-down SEM images of PS-*b*-PMMA (95k-*b*-92k) 25-nm-thick films annealed in acetone vapor for 46 h on striped chemical patterns with L_S = 60-90 nm.

The shape of assembled hexagons and the order of their assembled structure reflected the commensurability of L_S with $L_{0,s}$. Long-range-ordered hexagonal patterns of PS hexagons assembled on the chemical patterns with L_S = 70, 75, and 80 nm (Fig. 4c-e). The PS hexagons were nearly symmetric at L_S = 70 and 75 nm, although they were smaller when L_S = 70 nm. When L_S = 65 nm, the PS hexagons were stretched in the direction of the chemical pattern stripes, and defects were apparent in the ordering of the domains. The defects in hexagonal domain shape and ordering were more pronounced when L_S was decreased to 60 nm. In contrast to the assemblies when L_S = 65 nm, when L_S = 80 nm the PS hexagons stretched in the direction normal to the chemical pattern stripes. When L_S > 80 nm symmetric hexagons formed patterns with the period between lines of assembled hexagons approximately equal to $L_{0,s}$, without long-range ordering on the chemical patterns. In all cases, the hexagonally shaped PS domains became more circular when the PMMA was removed (Supporting Information Figure S2).

DSA of Stripes on Non-Regular Chemical Patterns (Bends). We also investigated DSA of PS-*b*-PMMA (95k-*b*-92k) ultrathin films on nonregular chemical patterns in the form of bends. Figure 5 shows the top-down SEM images of 25-nm-thick PS-*b*-PMMA films assembled on nested arrays of lines (L_S = 75 nm) with either 60°, 90°, 120°, or 150° bends. The PS-*b*-PMMA films were annealed in acetone vapor for 10 h. DSA with high perfection was observed on the linear portions of the chemical patterns. At the point of the bend, the corner-to-corner period, L_c, increases with bend angle, θ (inset in Fig. 5a). The corner-to-corner period, $L_c = L_S/\cos(\theta/2)$, is 86.6, 106.1, 150, and 289.8 nm for 60°, 90°, 120°, and 150° bends, respectively. Defects at the corner were expected when L_c was larger than the largest L_S of chemical patterns that directed nearly perfect assembly of stripes (85 nm, Fig. 3), corresponding to θ > 60°. However, using solvent annealing, defect-free DSA was observed on chemical patterns with 60°, 90°, 120° bends (Fig. 5a-c). Similar results were demonstrated in our group by DSA with thermal annealing of ternary blends of symmetric PS-*b*-PMMA and their corresponding homopolymers (PS and PMMA).[9] In that earlier work, the formation of the defect-free assembly at the bends was facilitated by the redistribution of homopolymers. Here, we believe that the adsorbed solvent played a similar role.

DSA of Stripes with Density Multiplication. DSA of ~20-nm-thick films of symmetric PS-*b*-PMMA (52k-*b*-52k) on 1:2 chemical patterns *via* solvent annealing was also demonstrated, as shown in Figure 6. We fabricated well-defined 1:2 chemical patterns that consisted of XPS stripes with $0.5L_{0,s}$ in width and backfilled with $PS_{57\%}$-*r*-PMMA-OH in the interspatial regions.[47] After 1.5 h of annealing PS-*b*-PMMA in acetone vapor, both PMMA dots and stripes were observed, and 5 h of annealing resulted in stripe structures (Supporting Information Figure S3). The assembly required less time than for the higher M_n (95k-*b*-92k) PS-*b*-PMMA. The stripes of PS-*b*-PMMA (52k-*b*-52k) on the PS-OH grafted silicon substrate had $L_{0,s}$ = 41 nm. As a result, the 80-nm chemical pattern directed nearly perfect assembly of the stripes with two-fold density multiplication (Fig. 6c). On chemical patterns with L_S = 70, and 90 nm (Fig. 6b and d), only a small portion of the BCP stripes registered to the stripes of the underlying chemical pattern. When L_S and $2L_{0,s}$ were very incommensurate (L_S = 100 nm) a disordered, fingerprint pattern was observed (Fig. 6e).

Discussion

The shapes formed during self-assembly and DSA in Figure 1 can be understood in terms of the mechanism of the self-assembly of the domains. The mechanism of assembly in this work appears to be dominated by two factors: the thinness of the film and the migration of PMMA chains from the bottom to the top surface.[38, 40] Initially, the as-cast films have a PS-rich layer at the top

surface due to the lower surface energy of PS, compared to PMMA, at room temperature. The presence of PS at the free surface was verified by the measureement of the water contact angle (88°) of the as-cast film. After 1.5 h of exposure to acetone vapor the contact angle dropped to ~68°, indicating that PMMA was dominating the top surface. The migration of PMMA to the top surface, and the initial reorginization of the PS-*b*-PMMA, effectively erased what little morphology was evident at the top surface of the as-cast films. The presence of acetone vapor, a PMMA-selective solvent, made it more preferable to have a PMMA wetting layer than a PS wetting layer on the top surface. As more PMMA block rises to the top surface, the top surface forms structures that contain more and more PMMA. Thus, after 5 h of solvent annealing, solid black spots of PMMA are present, which were not present after 1.5 h. It is likely these dots represent the tips of truncated cones of PMMA, similar to the morphology proposed by Xuan *et al*.[40] As the annealing continues, structures that contain progressively more PMMA appear: PMMA stripes, and then PS hexagons. We refer to the PMMA stripes as "stripes" and not "lamellae" because SEMs show that after removal of PMMA, there are some thin PS bridges between PS domains (Supporting Information Figures S2 and S4.) The progression of morphologies shown here is similar to the observations of Xuan *et al*.[40] However, less time was required for structural formation and change in this work compared to theirs because M_n of our PS-*b*-PMMA was lower than theirs. The significance of the PMMA migration to the top surface can also explain why the morphological evolution behavior is independent of substrate chemistry (Supporting Information Figure S2).

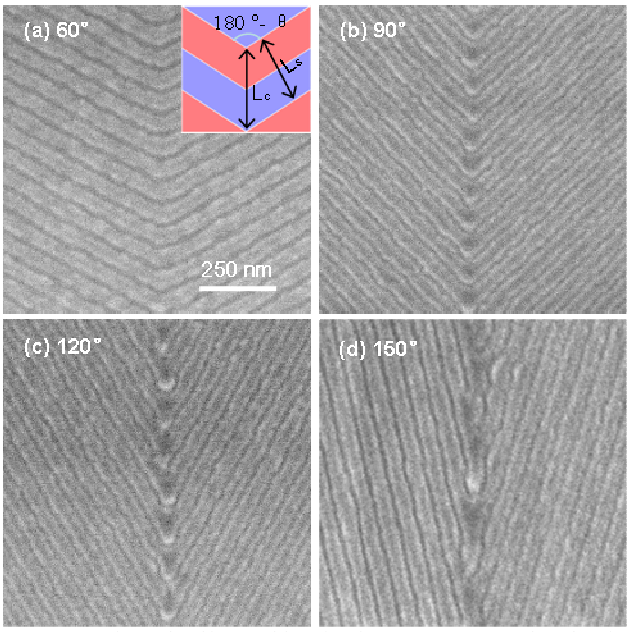

Figure 5. Directed self-assembly of stripes on a non-regular chemical pattern. Top-down SEM images of PS-*b*-PMMA (95k-b-92k) 25-nm-thick films annealed in acetone vapor for 10 h on chemical patterns with L_S = 75 nm and bend angle θ = 60° (a), 90° (b), 120° (c), and 150° (d).

The thinness of the film (thickness < $0.5L_0$) is important because it prevents the formation of a surface-parallel lamellae morphology, which would normally occur for a BCP film on a homogeneous, preferentially wetting substrate such as PS-OH or PMMA-OH brush. However, in this work because the film thickness is less than $0.5L_0$, formation of surface-parallel lamellae would require significant compression of the polymer chains, which would be entropically unfavorable.[48] Instead, the progression of non-bulk morphologies described above form sequentially. The contact angles of these films were all approximately 80°, indicating the coexistence of both PS and PMMA blocks on the top surfaces.

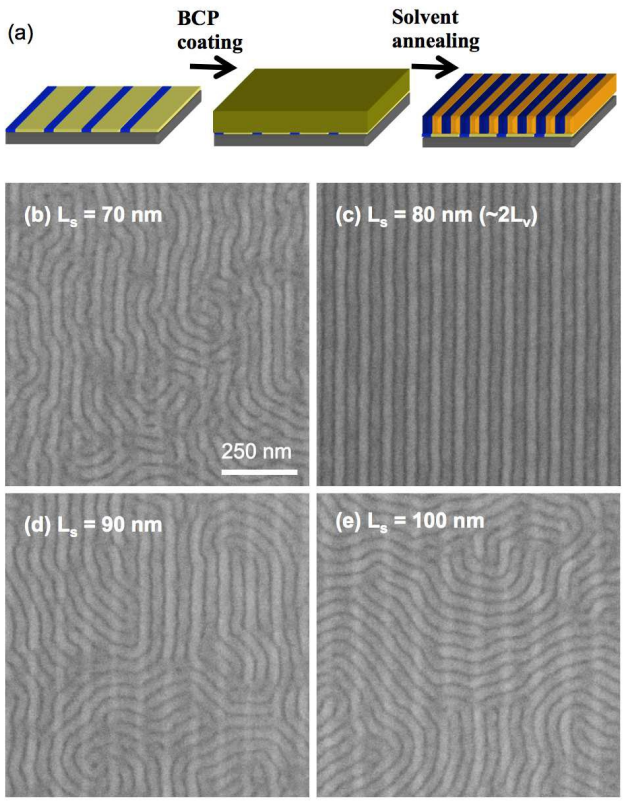

Figure 6. (a) Schematic of the solvent-annealing-induced two-fold density multiplication on chemical patterns. (b-e) Top-down SEM images of PS-*b*-PMMA (52k-*b*-52k) 25-nm-thick films on chemical patterns with L_S = 70-100 nm after being annealed in acetone vapor for 5 h.

The mechanism of the evolution of the morphology of the PS-*b*-PMMA as it assembles in the acetone vapor appears to differ from some assembly mechanisms presented in earlier work. In one previous study, the evolution of surface morphologies of asymmetric polystyrene-*block*-poly(4-vinylpyridine) (PS-*b*-P4VP) thin film (thickness ~ L_0) on a silicon substrate annealed in THF vapor was investigated.[49] In that work, no geometry change was observed with increasing annealing time, but the distribution of the size and period of the cylindrical microdomains significantly narrowed. The change in the size and period of the domains was associated with the swelling ratio and dynamics of the PS-*b*-P4VP. Wang *et al*.[50] studied the morphological evolution in thin films (thickness ~ L_0) of asymmetric polystyrene-*block*-poly(ethylene/butylene)-*block*-polystyrene annealed in cyclohexane vapor, a selective solvent for the majority poly(ethylene/butylene) block. Atomic force microscopy scanning results on *ex situ* annealed films suggested that the

phase separation along with increasing annealing time consisted of two sequential steps: 1) the cyclic transition between poorly ordered cylinders and semidisordered cylinders *via* poorly ordered spheres, 2) the pinching-off from partially ordered cylinders into hexagonally close packed spheres.

In thermally annealed BCP thin films with thicknesses less than L_0, non-bulk morphologies have also been demonstrated both in experiment and in theory.[48, 51, 52] For instance, half lamellae, perpendicular lamellae, hybrid structures, and anti-symmetric hybrid structures were predicted and observed in thermally-annealed symmetric diblock copolymer films with thickness ~$0.5L_0$.[48] These non-bulk morphologies were typically observed at the edge of a discontinuous film[51, 53] with local thickness variations. Generally they were not suitable for lithographic applications because the formation of uniform patterns demanded undesired substrate modifications.[54]

When BCP films are solvent annealed, microdomain structures and their ordering may form during solvent evaporation following the "nucleation-and-growth" mechanism[55] or in the solvated state following the "quasi-equilibrium-and-quenching" mechanism.[56] In the "nucleation-and-growth" mechanism, the BCP thin film is disordered in the swollen state. Solvent evaporation at the free surface drives the nucleation of ordered microdomain structures. The ordering front propagates downward through the film as solvent evaporation continues. In contrast, we observed that the ordering of the BCP thin films is guided by underlying chemical patterns. The solvent annealing presented here can be better described by the "quasi-equilibrium-and-quenching" mechanism, in which microdomains form in the swollen state, and the assembled structure is retained after rapid removal of solvent from the film, except with compression in the direction normal to the substrates during solvent removal.

The similarities of the results of DSA with solvent annealing shown here with previous results from studies of DSA with thermal annealing provide strong evidence that in solvent annealing assembly occurs in the solvated but microphase separated state. Solvated microphase separated domains form a characteristic period, $L_{0,s}$, based on a balance of interfacial energy between domains and chain configurational energy wtihin the domains. That energy balance is perturbed when assembled in a thin film in the presence of a chemical pattern. For example, the ability of DSA with solvent annealing to achieve a pattern period equal to L_S, provided that L_S is close in value to $L_{0,s}$, is directly analogous to the thermal annealing DSA results of Edwards *et al*., which showed that perfect assembly of thin films of symmetric PS-*b*-PMMA on striped patterns could be achieved with assembled periods equal to L_S provided that $L_S = L_0 \pm 10\%$, where L_0 is the bulk period of the block copolymer.[6] Edwards *et al*. used well-known expressions for surface energy, domain interfacial energy, and chain configurational energy to show that DSA of the domains will occur over incommensurate substrates ($L_S \neq L_0$) as long as the energy savings provided by the domain spacing matching L_S exceeds the energy penalty of the chain deformation required to match L_S. In this work the commensurability window of at least ±7% is centered about $L_{0,s}$, showing that the assembly of the domains occurs in the solvated state, again balancing the energy required for chain deformation when $L_S \neq L_{0,s}$ with the energy provided by the assembled domain period matching L_S.

Further proof is offered by the similarity of the deformation of PS hexagons when $L_S \neq L_{0,s}$ in this work with the deformation of assembled cylinders observed by Park *et al*. in thin films of PS-*b*-PMMA that were thermally annealed on chemical patterns incommensurate with L_0 of their BCP.[57] Similarly, Cheng *et al*. reported on the elliptical distortion of spherical domains of polystyrene-*block*-polyferrocenyldimethylsilane that were assembled via thermal annealing in topographical trenches designed with widths incommensurate to L_0 of the spherical domains.[58] Both of these works showed that cylindrical or spherical domains assembled on substrates with dimensions incommensurate with the charatcteristic dimensions of the BCP can adjust their domain shape to minimize the chain configurational energy penalty associated with assembly on an incommensurate substrate. In an analogous way, in this work, the solvated PS hexagons adjusted their domain shape to minimize the entropic penalty associated with assembly on a substrate with $L_S \neq L_{0,s}$.

The formation of PS hexagons, as opposed to PS cylinders or spots, reveals the influence of acetone on the final morphology. Normally hexagonal domains are not apparent in diblock copolymer systerms, but Thomas's group has demonstrated hexagonal domains with ABC block copolymers[59, 60] and terpolymers.[61] In pure, cylinder-forming diblock copolymers, the minority domains have a preference for a hexagonal structure to create more uniform chain stretching of the majority block in the hexagonal Wigner-Seitz cells[62] but this desire is outweighed by the need to minimize domain interfacial surface area resulting in the formation of cylinders.[63] In this work it seems that the acetone decreases the influence of the domain interfacial surface area minimization, thereby enabling the PS domains to assume a hexagonal shape, which was retained after the acetone was rapidly evaporated.

Besides the ordered and naturally occurring patterns, such as parallel lines and close packed dots, data storage and semiconductor industries also demand more complicated, non-regular structures from BCP. Solvent annealing has shown its significant advantages over thermal annealing on tailoring the geometries and sizes of the BCP patterns. Compared to BCP blocks, the solvent molecules are much smaller, and therefore have more freedom to rearrange during phase separation. The rearrangement may help the assembly of some non-regular structures, e.g. bends (Fig. 5). In Fig. 5, the darker color in the corner of the bends indicates depressions in the local film that were caused by those regions having a larger fraction of solvent in solvated state than regions away from the corners. It is worth noting that such surface topography may cause complications in subsequent etching processes.

DSA of these non-bulk microdomains on chemical patterns has been realized with and without density multiplication. In both cases, assemblies yield long-range-ordered, uniform, two-dimensional (2D) patterns based on top-down SEM images (Fig. 1-6). However, for the application of nanolithography, the pattern quality has to be determined in a three-dimensional (3D) manner. Generally, perpendicularly oriented structures that traverse the the thickness of the film are favored for subsequent pattern transfer. In Supporting Information Fig. S2 (middle row) and Fig. S4, the PMMA blocks were removed by acetic acid after UV

exposure. The high contrast between the remaining PS block and the voids caused by PMMA removal implies that all three types of structures are perpendicular through the whole film thickness. This 3D morphology was also verified by imaging the backside of the film.[39] We noticed that the morphologies we observed differed from standard bulk morphologies. In Fig. S2 (middle row) and Fig. S4, the PS residue inside the trenches indicates the stripes are not typical perpendicular lamellae. The unusually large size of the PS hexagons, not to mention their hexagonsal shape, suggests that they are not the standard spherical morphology.

Conclusions

In summary, we have demonstrated that DSA on chemical patterns of a BCP in the vapor of a selective solvent can yield ordered, registered patterns of a variety non-bulk BCP morphologies provided that the period of the chemical pattern L_S is close to commenurate with $L_{0,s}$ of the solvated BCP. The similarities between the solvent annealing results presented her provide compelling evidence that the assemblies observed after solvent annealing were formed while the BCP was in the solvated state. Unlike previous work on DSA, which focused on equilibrated BCP microdomains, this work extends DSA to non-equilibrium BCP microdomains. Control of structure formation is provided, in part, by the amount of time the BCP film is permitted to anneal in solvent vapor. As such, patterns with various geometries can be obtained from a single BCP/solvent system. We have also shown that solvent annealing may have advantages over thermal annealing on the formation of device-oriented non-regular structures.

Acknowledgments

This work is supported by the U.S. Department of Energy, Office of Science, Office of Basic Energy Sciences-Materials Science. SJ acknowledges the financial support from the National Natural Science Foundation of China (Nos. 51173181, 51373166) and "The Hundred Talents Program" from the Chinese Academy of Sciences.

Notes and references

[a] *HGST, a Western Digital Company, San Jose Research Center, 3403 Yerba Buena Rd., San Jose CA 95135*
[b] *Key Laboratory of Polymer Ecomaterials, Changchun Institute of Applied Chemistry, Chinese Academy of Science, 5625 Renmin Street, Changchun, 130022 China*
[c] *IBM Albany NanoTech, 257 Fuller Road, Albany NY 12203*
[d] *Institute for Molecular Engineering, University of Chicago, 5747 South Ellis Avenue, Chicago, IL 60637 USA. Tel: (773) 702-9143; E-mail: nealey@uchicago.edu*

† Electronic Supplementary Information (ESI) available: Fig. S1-S4. See DOI: 10.1039/b000000x.

1. H.-C. Kim, S.-M. Park and W. D. Hinsberg, *Chemical Reviews*, 2010, **110**, 146-177.
2. M. A. Morris, *Microelectron. Eng.*, 2015, **132**, 207-217.
3. J. Bang, U. Jeong, D. Y. Ryu, T. P. Russell and C. J. Hawker, *Adv. Mater.*, 2009, **21**, 4769-4792.
4. F. S. Bates and G. H. Fredrickson, *Annu. Rev. Phys. Chem.*, 1990, **41**, 525-557.
5. S. Xiao, X. Yang, S. Park, D. Weller and T. P. Russell, *Adv. Mater.*, 2009, **21**, 2516-2519.
6. E. W. Edwards, M. F. Montague, H. H. Solak, C. J. Hawker and P. F. Nealey, *Adv. Mater.*, 2004, **16**, 1315-1319.
7. E. W. Edwards, M. P. Stoykovich, M. Müller, H. H. Solak, J. J. De Pablo and P. F. Nealey, *J. Polym. Sci., Part B: Polym. Phys.*, 2005, **43**, 3444-3459.
8. S. O. Kim, H. H. Solak, M. P. Stoykovich, N. J. Ferrier, J. J. de Pablo and P. F. Nealey, *Nature*, 2003, **424**, 411-414.
9. M. P. Stoykovich, M. Müller, S. O. Kim, H. H. Solak, E. W. Edwards, J. J. de Pablo and P. F. Nealey, *Science*, 2005, **308**, 1442-1446.
10. R. Ruiz, H. Kang, F. A. Detcheverry, E. Dobisz, D. S. Kercher, T. R. Albrecht, J. J. de Pablo and P. F. Nealey, *Science*, 2008, **321**, 936-939.
11. I. Bita, J. K. W. Yang, Y. S. Jung, C. A. Ross, E. L. Thomas and K. K. Berggren, *Science*, 2008, **321**, 939-943.
12. X. M. Yang, L. Wan, S. G. Xiao, Y. A. Xu and D. K. Weller, *ACS Nano*, 2009, **3**, 1844-1858.
13. Y. Tada, S. Akasaka, H. Yoshida, H. Hasegawa, E. Dobisz, D. Kercher and M. Takenaka, *Macromolecules*, 2008, **41**, 9267-9276.
14. J. Y. Cheng, C. T. Rettner, D. P. Sanders, H. C. Kim and W. D. Hinsberg, *Adv. Mater.*, 2008, **20**, 3155-3158.
15. R. A. Segalman, H. Yokoyama and E. J. Kramer, *Adv. Mater.*, 2001, **13**, 1152-1155.
16. J. Y. Cheng, C. A. Ross, E. L. Thomas, H. I. Smith and G. J. Vancso, *Appl. Phys. Lett.*, 2002, **81**, 3657-3659.
17. J. Y. Cheng, A. M. Mayes and C. A. Ross, *Nat. Mater.*, 2004, **3**, 823-828.
18. S. G. Xiao, X. M. Yang, E. W. Edwards, Y. H. La and P. F. Nealey, *Nanotechnology*, 2005, **16**, S324-S329.
19. T. R. Albrecht, H. Arora, V. Ayanoor-Vitikkate, J.-M. Beaujour, D. Bedau, D. Berman, A. L. Bogdanov, Y.-A. Chapuis, J. Cushen, E. E. Dobisz, G. Doerk, H. Gao, M. Grobis, B. Gurney, W. Hanson, O. Hellwig, T. Hirano, P.-O. Jubert, D. Kercher, J. Lille, Z. Liu, C. M. Mate, Y. Obukhov, K. C. Patel, K. Rubin, R. Ruiz, M. Schabes, L. Wan, D. Weller, T.-W. Wu and E. Yang, *IEEE Trans. Magn.*, 2015, **51**, 0800342.
20. O. Hellwig, J. K. Bosworth, E. Dobisz, D. Kercher, T. Hauet, G. Zeltzer, J. D. Risner-Jamtgaard, D. Yaney and R. Ruiz, *Appl. Phys. Lett.*, 2010, **96**, 052511.
21. C. T. Black, R. Ruiz, G. Breyta, J. Y. Cheng, M. E. Colburn, K. W. Guarini, H. C. Kim and Y. Zhang, *IBM J. Res. Dev.*, 2007, **51**, 605-633.
22. J. Y. Cheng, D. P. Sanders, H. D. Truong, S. Harrer, A. Friz, S. Holmes, M. Colburn and W. D. Hinsberg, *ACS Nano*, 2010, **4**, 4815-4823.
23. C. Bencher, J. Smith, L. Miao, C. Cai, Y. Chen, J. Y. Cheng, D. P. Sanders, M. Tjio, H. D. Truong, S. Holmes and W. D. Hinsberg, *Proc. SPIE, Alternative Lithographic Technologies III*, 2011, **7970**, 79700F-79700F.
24. C. Sinturel, M. Vayer, M. Morris and M. A. Hillmyer, *Macromolecules*, 2013, **46**, 5399-5415.
25. J. K. Bosworth, M. Y. Paik, R. Ruiz, E. L. Schwartz, J. Q. Huang, A. W. Ko, D. M. Smilgies, C. T. Black and C. K. Ober, *ACS Nano*, 2008, **2**, 1396-1402.
26. Y. S. Jung and C. A. Ross, *Adv. Mater.*, 2009, **21**, 2540-2545.
27. J. W. Jeong, W. I. Park, M.-J. Kim, C. A. Ross and Y. S. Jung, *Nano Lett.*, 2011, **11**, 4095-4101.
28. M. A. Chavis, D.-M. Smilgies, U. B. Wiesner and C. K. Ober, *Adv. Funct. Mater.*, 2015, **25**, 3057-3065.
29. S. Park, D. H. Lee, J. Xu, B. Kim, S. W. Hong, U. Jeong, T. Xu and T. P. Russell, *Science*, 2009, **323**, 1030-1033.
30. S. Park, J. Y. Wang, B. Kim, J. Xu and T. P. Russell, *ACS Nano*, 2008, **2**, 766-772.
31. T. P. Russell, S. W. Hong, X. D. Gu, J. Huh and S. G. Xiao, *ACS Nano*, 2011, **5**, 2855-2860.
32. V. P. Chuang, J. Gwyther, R. A. Mickiewicz, I. Manners and C. A. Ross, *Nano Lett.*, 2009, **9**, 4364-4369.
33. L. S. Wan, P. A. R. Delgadillo, R. Gronheid and P. F. Nealey, *J. Vac. Sci. Technol., B*, 2013, **31**, 06F301.
34. J. K. Bosworth, E. Dobisz and R. Ruiz, *J. Photopolym. Sci. Technol.*, 2010, **23**, 145-148.

35. Y. Tada, H. Yoshida, Y. Ishida, T. Hirai, J. K. Bosworth, E. Dobisz, R. Ruiz, M. Takenaka, T. Hayakawa and H. Hasegawa, *Macromolecules*, 2012, **45**, 292-304.
36. J. Xu, S. W. Hong, W. Y. Gu, K. Y. Lee, D. S. Kuo, S. G. Xiao and T. P. Russell, *Adv. Mater.*, 2011, **23**, 5755-5761.
37. Y.-H. Wu, T.-Y. Lo, M.-S. She and R.-M. Ho, *ACS Applied Materials & Interfaces*, 2015, **7**, 16536-16547.
38. J. Peng, D. H. Kim, W. Knoll, Y. Xuan, B. Li and Y. Han, *J. Chem. Phys.*, 2006, **125**, 064702.
39. J. Peng, Y. Xuan, H. F. Wang, Y. M. Yang, B. Y. Li and Y. C. Han, *J. Chem. Phys.*, 2004, **120**, 11163-11170.
40. Y. Xuan, J. Peng, L. Cui, H. F. Wang, B. Y. Li and Y. C. Han, *Macromolecules*, 2004, **37**, 7301-7307.
41. M. P. Stoykovich, H. Kang, K. C. Daoulas, G. Liu, C. C. Liu, J. J. de Pablo, M. Mueller and P. F. Nealey, *ACS Nano*, 2007, **1**, 168-175.
42. G. Liu, C. S. Thomas, G. S. W. Craig and P. F. Nealey, *Adv. Funct. Mater.*, 2010, **20**, 1251-1257.
43. S. X. Ji, U. Nagpal, G. L. Liu, S. P. Delcambre, M. Muller, J. J. de Pablo and P. F. Nealey, *ACS Nano*, 2012, **6**, 5440-5448.
44. R. Ruiz, H. M. Kang, F. A. Detcheverry, E. Dobisz, D. S. Kercher, T. R. Albrecht, J. J. de Pablo and P. F. Nealey, *Science*, 2008, **321**, 936-939.
45. P. Mansky, Y. Liu, E. Huang, T. P. Russell and C. J. Hawker, *Science*, 1997, **275**, 1458-1460.
46. H. H. Solak, C. David, J. Gobrecht, V. Golovkina, F. Cerrina, S. O. Kim and P. F. Nealey, *Microelectron. Eng.*, 2003, **67-8**, 56-62.
47. C. C. Liu, E. Han, M. S. Onses, C. J. Thode, S. X. Ji, P. Gopalan and P. F. Nealey, *Macromolecules*, 2011, **44**, 1876-1885.
48. M. J. Fasolka, P. Banerjee, A. M. Mayes, G. Pickett and A. C. Balazs, *Macromolecules*, 2000, **33**, 5702-5712.
49. S. Park, B. Kim, J. Xu, T. Hofmann, B. M. Ocko and T. P. Russell, *Macromolecules*, 2009, **42**, 1278-1284.
50. Y. Wang, X. Hong, B. Liu, C. Ma and C. Zhang, *Macromolecules*, 2008, **41**, 5799-5808.
51. A. Knoll, A. Horvat, K. S. Lyakhova, G. Krausch, G. J. A. Sevink, A. V. Zvelindovsky and R. Magerle, *Phys. Rev. Lett.*, 2002, **89**, 035501.
52. H. P. Huinink, J. C. M. Brokken-Zijp, M. A. van Dijk and G. J. A. Sevink, *J. Chem. Phys.*, 2000, **112**, 2452-2462.
53. T. L. Morkved and H. M. Jaeger, *Europhys. Lett.*, 1997, **40**, 643-648.
54. M. J. Fasolka, D. J. Harris, A. M. Mayes, M. Yoon and S. G. J. Mochrie, *Physical Review Letters*, 1997, **79**, 3018-3021.
55. S. H. Kim, M. J. Misner and T. P. Russell, *Adv. Mater.*, 2004, **16**, 2119-2123.
56. M. Y. Paik, J. K. Bosworth, D. M. Smilges, E. L. Schwartz, X. Andre and C. K. Ober, *Macromolecules*, 2010, **43**, 4253-4260.
57. S. M. Park, G. S. W. Craig, C. C. Liu, Y. H. La, N. J. Ferrier and P. F. Nealey, *Macromolecules*, 2008, **41**, 9118-9123.
58. J. Y. Cheng, F. Zhang, V. P. Chuang, A. M. Mayes and C. A. Ross, *Nano Lett.*, 2006, **6**, 2099-2103.
59. S. P. Gido, D. W. Schwark, E. L. Thomas and M. do Carmo Goncalves, *Macromolecules*, 1993, **26**, 2636-2640.
60. R. L. Lescanec, L. J. Fetters and E. L. Thomas, *Macromolecules*, 1998, **31**, 1680-1685.
61. S. Sioula, N. Hadjichristidis and E. L. Thomas, *Macromolecules*, 1998, **31**, 5272-5277.
62. G. M. Grason, *Physics Reports-Review Section of Physics Letters*, 2006, **433**, 1-64.
63. M. W. Matsen and F. S. Bates, *J. Chem. Phys.*, 1997, **106**, 2436-2448.

Directed Self-Assembly of Solvent-Vapor-Induced Non-Bulk Block Copolymer Morphologies on Nanopatterned Substrates

Lei Wan, Shengxiang Ji, Chi-Chun Liu, Gordon S.W. Craig, and Paul F. Nealey

We demonstrate that annealing a thin film of block copolymer in the vapor of a solvent that is selective to one of the blocks can yield block copolymer domains that do not naturally occur in the bulk, and that these domains can be aligned with and registered to an underlying chemical pattern.

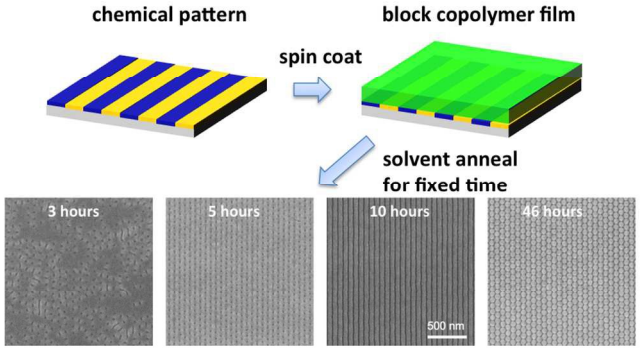

508x381mm (72 x 72 DPI)